
Steering polymer growth by molding nanochannels: 1,5-hexadiene polymerization in high silica mordenite.

Marco Fabbiani^{[a],[b]}, Giorgia Confalonieri^[c], Sara Morandi^{[a],[b]}, Rossella Arletti^{[c]*}, Simona Quartieri^[c], Mario Santoro^[d], Francesco Di Renzo^[e], Julien Haines^[e], Riccardo Fantini^[c], Gloria Tabacchi^{*[f]}, Ettore Fois^[f], Giovanna Vezzalini^[c], and Gianmario Martra^{[a],[b]*}

- [a] Dr. M. Fabbiani, Dr. S. Morandi, Prof. Dr. G. Martra
Dipartimento di Chimica
Università degli Studi di Torino
Via Pietro Giuria 7, 10125 Torino, Italy
E-mail: gianmario.martra@unito.it
- [b] Dr. M. Fabbiani, Dr. S. Morandi, Prof. Dr. G. Martra
Interdepartmental Centre "Nanostructured Interfaces and Surfaces" - NIS
Università degli Studi di Torino
Via Pietro Giuria 7, 10125 Torino, Italy
- [c] Dr. G. Confalonieri, Dr. R. Fantini, Prof. Dr. R. Arletti, Prof. Dr. S. Quartieri, Prof. Dr. G. Vezzalini,
Dipartimento di Scienze Chimiche e Geologiche
Università degli Studi di Modena e Reggio Emilia
Via Campi 103, 41125 Modena, Italy
E-mail: rossella.arletti@unimore.it
- [d] Dr. M. Santoro
Istituto Nazionale di Ottica, CNR-INO, and European Laboratory for Non Linear Spectroscopy LENS
Via Nello Carrara 1, 50019 Sesto Fiorentino, Italy
- [e] Dr. J. Haines, Dr. F. Di Renzo
ICGM, Univ. Montpellier, CNRS, ENSCM, Montpellier, France
Place Eugène Bataillon, 34095 Montpellier, France
- [f] Prof. Dr. G. Tabacchi, Prof. Dr. E. Fois
Dipartimento di Scienza ed Alta Tecnologia and INSTM
Università degli Studi dell'Insubria
Via Valleggio 11, 22100 Como, Italy
E-mail: gloria.tabacchi@uninsubria.it

Supporting information for this article is given via a link at the end of the document.

Abstract: Zeolites are known as scaffolds for the assembly of molecules via non-covalent interactions, yielding organized supramolecular materials. Yet their potential in driving the growth of low-dimensional systems requiring covalent bond formation is still uncharted. We incorporated 1,5-hexadiene in the channels of a high-silica mordenite and analyzed the material by infrared spectroscopy, X-Ray powder diffraction, thermogravimetric and modeling techniques. Thanks to the few zeolite acid sites, 1,5-hexadiene experiences a slow conversion to a polymer, mainly formed by cyclopentane units and featuring short side chains able to fit the channels. The shape-directing abilities of zeolite framework play a two-fold role, involving first the organization of the monomers inside the void-space and then the linear growth of the chain, dictated by the channel geometry. These findings highlight the molding action of zeolites in directing transformations of covalent bonds under ambient conditions and may provide insights for obtaining confined polymers with intriguing perspective applications.

Introduction

The organization of objects, like molecules or clusters, in low-dimensionality nanosized structures is the key to attain materials endowed with new functionalities.^[1-4] This leitmotiv in advanced material science often relies on spontaneous assembly mechanisms - such as molecular recognition or intermolecular interactions - which could be enhanced or accelerated by imparting proper external stimuli *e.g.* via electromagnetic fields,^[5]

chemical reagents, or by imposing geometric restrictions.^[3,6-10] In the latter instance, materials exhibiting empty nanospace arrays are especially attractive because their pores can be exploited as nanosized receptors for the matter to create confined, supramolecular structures with low-dimensionality.^[11] The preparation and exploitation of low-dimensionality materials is still a fundamental issue in nanoscience and nanotechnology. Microporous materials such as zeolites are of great interest in this context because of their unique pore topologies.^[12] The "open space" of zeolites can be filled by suitable encapsulated guest molecules and cations, that can diffuse in the pores and organize in low-dimensional aggregates tailored by zeolite channels.^[13-15] Moreover, the fine tuning of their pore architecture and their hydrophilic/hydrophobic character can improve their performance for technological or industrial applications.^[4,16-24] The geometrical constraints of the zeolitic framework can be proficiently exploited to induce the formation of nanostructured arrays with the desired dimensionality. Supramolecular materials which do not require chemical reactions to form composites - such as dye-zeolite composites/artificial antenna systems in zeolite channels,^[25-33] biomolecules and chromophores immobilized in 1-D channels,^[34-41] or low-dimensional nano-architectures of molecular clusters^[42-44] - have been successfully realized. The preparation of a continuous organic nanowire via a chemical reaction, *i.e.* polymerization reaction, would be of fundamental relevance in advanced materials fabrication. In fact, preparing isolated, self-standing, densely packed polymers, is extremely challenging when conventional protocols are adopted, since the aggregation and bending of chains prevent the

production of real 1D systems.^[45,46] A possible solution could be the use of large-pore matrices as “microvessels” for conducting the polymerization reaction – such as mesoporous silicas/organosilicas^[47,48] and MOFs.^[49] On the other hand, zeolite cavities would be more suitable for small monomers, as the stricter space confinement might increase the degree of control on the polymer’s structure.^[50,51] Indeed, by imposing pressure on zeolite systems, it is possible to induce a rearrangement of the chemical bonds among guest species hosted in the pores by purely mechanical tuning the intermolecular/interatomic distances via relatively high pressures (few GPa). Following this procedure, linear chains of polyethylene,^[52] polyacetylene^[53] and polycarbonyl^[54] were synthesized inside zeolite channels and, very recently, phenylacetylene was oligomerized at high pressure inside the zeolite Mordenite (MOR).^[55] Differently, the formation of mixtures of long-chain polymers and small oligomers of pyrrole and thiophene were reported to occur inside transition-metal substituted zeolites, such *e.g.* Cu- or Ni- mordenites.^[56,57] Also, the presence of Brønsted acid sites^[58–65] could strongly affect the formation of a polymer inside the zeolite cavities: in particular, acid zeolites themselves can induce a polymerization reaction without the need of using high pressure and/or transition metals as catalysts.^[46] Overall, despite such a long-standing interest, the field of polymer/zeolite nanocomposites remains underexplored and yet underexploited.^[66]

Mordenite zeolite (*HS-MOR*) (Figure 1a) – which can be viewed as formed by quasi-1D channels modulated by side pockets,^[67] while, as a flexible monomer, our choice falls on an α,ω -diene molecule – 1,5-hexadiene (also referred to as *hexa*, in the following) (Figure 1b). Indeed, in the absence of confinement, this molecule undergoes a series of complex reactions (*e.g.* Cope rearrangements,^[68] dimerizations,^[69] polymerizations^[70]) characterized by intricate paths leading to a mixture of products. A regular polymer, using 1,5-hexadiene as a monomer, can be obtained only via a homogeneous Ziegler-Natta catalyst, leading to the formation of poly(methylene-1,3-cyclopentane) (PMCP).^[71,72] Even using homogeneous Ziegler-Natta-type catalysts with chiral ligands, achieving full control over the polymerization products is by no means straightforward: not only four microstructures of maximum order are possible for PMCP^[70], but also the formation of cross-linked polymers has been reported.^[73] Overall, selectivity and polymer morphology strongly depend on both the catalyst and the process conditions.^[72,74,75] Hence, 1,5-hexadiene clearly represents a challenging test for the “space-confining” effectiveness of zeolite channels over the possible reaction products and their morphology. Indeed, while the capability of zeolites to impose a well-defined supramolecular arrangement by forcing relatively weak intermolecular interactions is well known, here we explore whether such “molding” effects might be effective in dealing with processes requiring transformations of strong covalent bonds, like in a polymerization reaction.

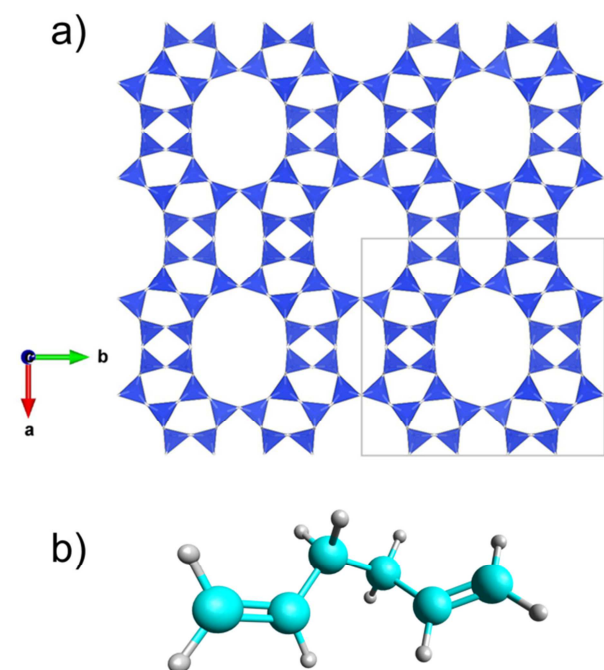


Figure 1. a) *HS-MOR* framework structure viewed along the [001] direction (the unit cell is drawn as grey solid lines); b) ball-and-stick representation of 1,5-hexadiene. The length and the maximum diameter of the 1,5-hexadiene molecule (inclusive of van der Waals radii) are 9.5 Å and 5.0 Å, respectively. (C=cyan; H=white).

Here we investigate the feasibility of mild conditions zeolite-induced polymerization adopting a highly flexible monomer in order to verify whether the zeolite channels shape could influence the structure of the final products. As host, we adopt a high silica

Results and Discussion

Basic investigation of the host steric constraints

The target of our work is to probe the shape-directing capability of the mordenite framework towards the controlled reaction among 1,5-hexadiene molecules within its regular, empty-space architecture. In particular, we want to see if such a confining matrix could force these non-conjugate diene molecules to form a polymer. In this case, the structure of the encapsulated polymer should be sterically compatible with the geometric restrictions of the *HS-MOR* channels. Hence the first step of our work is to inspect the mordenite framework to understand if 1,5-hexadiene based polymers could fit the zeolite mold.

The crystal structure of mordenite^[76] (framework type MOR^[77]) is built up from an assembly of single 6-membered rings (6MR) forming sheets linked by single 4-membered rings (4MR) or else from a combination of 5-1 secondary building units. As shown in Figure 1a, MOR exhibits a 1D channel system resulting from two types of channels both running parallel to the *c* axis: large 12MR channels (“free diameters” 6.5x7.0 Å) and strongly elliptic 8-membered rings (8MR) channels (“free diameters” 2.6x5.7 Å). These channels are interconnected along the [010] direction through side pockets delimited by 8MRs that, in turn, form a sinusoidal channel (“free diameters” 3.4 x4.8 Å) running parallel to the *b* axis. Only the main 12MR channels are accessible to hydrocarbon molecules. Mordenite has an orthorhombic unit cell with topological symmetry *Cmcm*. The real symmetry is reduced to *Cmc*₂^[78] thus avoiding a straight linkage between tetrahedral TO₄ units (T–O–T angle, T=Si, Al), but the crystal structure remains strongly pseudo-centrosymmetric.

The sample used in this work is a commercial synthetic high-silica mordenite (*HS-MOR*; *Si/Al=200*). The pristine material has been fully characterized and previously used in many studies, namely on the adsorption of pollutants from wastewaters,^[78-80] on the intrusion of ethylene glycol and water/alcohol mixtures at high pressure (HP)^[81] and in the oligomerization of phenylacetylene at HP.^[55] Structural data and relevant details of the Rietveld refinements on the pristine *HS-MOR* here used are reported in Table 1, as well as those of the synthesized host-guest compound *HS-MOR hexa*, later discussed (the final observed and calculated powder patterns for *HS-MOR hexa* are provided in the Supporting Information, Figure 1S; atomic coordinates, occupancy factors, thermal parameters and selected bond distances (Å) are reported in Tables 1S and 2S, respectively).

Table 1. Structural parameters of *HS-MOR* and *HS-MOR hexa* and refinement parameters of *HS-MOR hexa*.

	<i>HS-MOR</i> ^[a]	<i>HS-MOR hexa</i> ^[b]
Space group	<i>Cmcm</i>	<i>Cmcm</i>
a (Å)	18.0519(8)	18.0563(4)
b (Å)	20.2061(8)	20.2346(4)
c (Å)	7.4506(3)	7.4524(1)
V (Å ³)	2717.7(2)	2722.82(7)
H ₂ O molecules p.u.c. from refinement	3.6	3.5
R _{wp} (%)		5.32
R _p (%)		3.05
RF ² (%)		11.75
N _{obs}		854
N _{var}		71

[a] From Ref.^[81]. [b] This work.

The 1,5-hexadiene molecule (Figure 1b), which has a maximum diameter of 5.0 Å, is size-compatible with the 12MR channels and may be incorporated inside the *HS-MOR* framework. However, could 1-D oligomers/polymers composed by 1,5-hexadiene molecules be also compatible with the *HS-MOR* channels? To tackle this question, we considered the following models of continuous 1-D *hexa* polymers, depicted in Figure 2, which might all in principle fit to the 12MR channels:

- model A: a simple alkyl chain (of the poly(methylene) type), with no side moieties
- model B: a polymer with side chain constituted by a propyl group which penetrates inside the side pockets of MOR
- model C: a 1-D chain of (non-aromatic) 5-membered rings (cyclopentane), representative of a regular poly(methylene-1,3 cyclopentane) polymer
- model D: a chain containing cyclopentane units and lateral ethyl groups
- model E: a chain containing cyclopentane units and side vinyl groups.

The next step would be to examine whether any of these putative models could be representative of a low-

dimensionality polymer formed upon the incorporation of 1,5-hexadiene molecules in *HS-MOR*. We address this issue by means of multi-technique analyses, aimed at a closer characterization of the chemical features of the zeolite matrix.

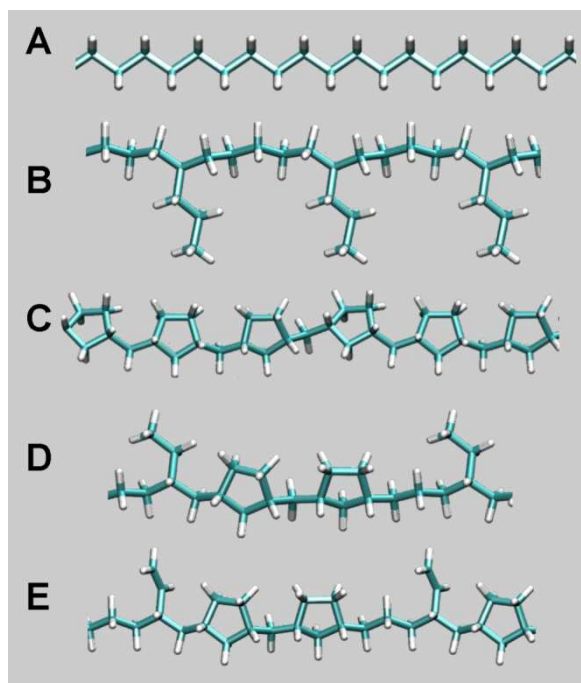


Figure 2. Graphical representation of the model 1-D-polymers A-E. Color codes: C=cyan; H=white.

Chemical features of *HS-MOR* as revealed by IR spectroscopy of adsorbed NH₃

In order to probe the chemical features of *HS-MOR*, the adsorption of NH₃ was carried out and monitored by IR spectroscopy. Figure 3 shows the spectra of *HS-MOR* outgassed at room temperature (r.t.), and in contact with NH₃ at the pressure of 2 mbar. As demonstrated in previous work,^[82] outgassing at r.t. (curve a) allowed the complete desorption of water molecules originally present in the zeolite channels, thus the signals present in the 3800-3000 cm⁻¹ range are overwhelmingly due to the νOH mode of silanols, framework Si-OH-Al and extraframework Al-OH species being a minor feature. Silanols involved in H-bonding, as in the so-called “silanol nests”, are responsible for the broad component spread over the 3650-3000 cm⁻¹ range (maximum out of scale), while SiOH involved in progressively weaker interactions produce the signals at higher frequency, with maxima at 3682 and 3730 cm⁻¹.

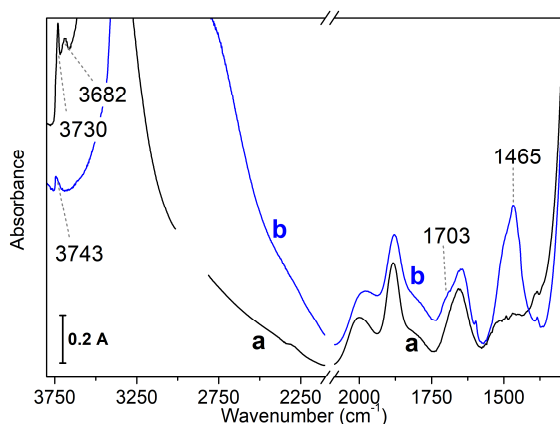


Figure 3. IR spectra of *HS-MOR*: a) after outgassing at r.t. for 1 h; b) after the admission of NH_3 , at $p = 2$ mbar.

Below 2000 cm^{-1} , a triplet is present, due to combinations (2000 and 1882 cm^{-1}) and an overtone (1654 cm^{-1}) of framework modes (absorbing below the low-frequency transparency limit imposed by the use of a self-supporting pellet, ca. 1300 cm^{-1}). The adsorption of NH_3 molecules (curve b) results in a change in the refractive index of the zeolite grains, with the consequent change in the scattering profile (different slope of the baseline, in a larger extent in the $3800\text{--}2400\text{ cm}^{-1}$ range). Focusing on the absorption spectral features, νOH signals due to silanols appeared downshifted, now contributing to a very broad and intense (maximum out of scale) absorption in the $3670\text{--}2400\text{ cm}^{-1}$ range, where also νNH components due to adsorbed NH_3 molecules should be present. The increase in the absorption intensity at about 1650 cm^{-1} is consistent with the appearance of an additional contribution due to the antisymmetric deformation mode of NH_3 molecules in interaction with silanols.^[83] Noteworthy, the main difference with respect to the spectrum of the bare zeolite is the appearance of components at 1703 (shoulder) and 1465 cm^{-1} , due to the deformation modes of NH_4^+ adducts, resulting from a proton transfer from the very minor canonical Si-OH-Al Brønsted sites possibly present and from silanols to adsorbed ammonia molecules. Indeed, cooperative effects occurring among SiOH in silanol nests have been proposed to increase the acidity of some silanols, becoming able to transfer their proton to sufficiently nucleophilic adsorbed molecules.^[84,85]

Reactivity of 1,5-hexadiene in *HS-MOR* as revealed by IR spectroscopy

The loading of 1,5-hexadiene in *HS-MOR* was monitored by *in situ* IR spectroscopy and the final sample was later used for thermogravimetry and the XRPD analyses.

Figure 4 shows the IR spectra of 1,5-hexadiene adsorbed on *HS-MOR* pre-outgassed at r.t. (curve a), and the subsequent evolution

as a function of contact time (curves b,c). The spectrum of the molecule in the gas phase (curve a') is reported for comparison. The assignment of the signals of the molecule in this form, as well as the beginning of the contact with *HS-MOR*, and along contact time is reported in Table 2. As a consequence of the interaction with the zeolite, the frequency of the modes producing signals in the accessible range is downshifted of few wavenumbers, but the main distinctive aspect is constituted by the appearance of additional bands at 1525 and 1380 cm^{-1} , and a shoulder at 1465 cm^{-1} . These signals are assignable to the C-C stretching of allylic carbocation species, the symmetric deformation mode ($\delta_s\text{CH}_3$) and the antisymmetric one ($\delta_{as}\text{CH}_3$) of $-\text{CH}_3$ groups, respectively.^[86,87] Partner C-H stretching modes of the methyl groups are expected at higher frequency, where they should contribute as minor, unresolved components to the spectral pattern in the $3000\text{--}2800\text{ cm}^{-1}$ range due to stretching modes of $-\text{CH}_2$ (sp^2) and $-\text{CH}_2$ (sp^3). The presence of these additional signals indicates that a proton transfer occurred from the zeolite to adsorbed molecules. Moreover, the formation of allyl carbocation species can be explained in terms of an initial protonation of one of the terminal C=C bonds, followed by a migration of the positive charge along the carbon atom chain towards the other terminal C=C, where the carbocations can experience resonance stabilization by delocalization of the positive charge to the adjacent π bond ($\text{R-C}(+)\text{H-CH=CH}_2 \leftrightarrow \text{R-CH=CH-C}(+)\text{H}_2$). Such a reactivity proceeded along the first hour of contact (curves b), as monitored by a decrease in intensity of the $\nu(\text{C}=\text{C})$ band (1641 cm^{-1}) and of signals related to $-\text{CH}_2$ (sp^2) (3083 , 2980 , 1417 cm^{-1}) and $-\text{CH}(\text{sp}^2)$ (3007 cm^{-1}), accompanied by an increase in the intensity of the band due to allylic carbocations (ca. 1525 cm^{-1}) and $-\text{CH}_3$ groups (2961 , 2873 , 1465 and 1380 cm^{-1}) (details on the assignment in Table 2). For longer contact time, the static condition entails the partial rehydration of the system by water molecules unavoidably remained adsorbed on the inner walls of the IR cell even after the initial outgassing at r.t., and H_2O stretching and bending modes interfere with the observation of the evolution of the $-\text{CH}_x$ (sp^2 and sp^3) and C=C signals (Figure 2S, see Supporting Information). After one week of contact, water molecules were removed by outgassing at r.t. and the whole spectral profile due to organic species became observable (curves c), revealing a strong decrease in intensity of the $-\text{CH}_2$ (sp^2) and $-\text{CH}(\text{sp}^2)$ signals, in favor of those due to $-\text{CH}_3$ groups. An evolution of the band assigned to allylic carbocations also occurred: the signal initially at 1525 cm^{-1} is converted in a complex pattern at lower frequency, constituted by at least three components, the most intense of them being located at 1498 cm^{-1} . Such a behavior can be due to some change in the interaction with the zeolite lattice, in terms of interaction strength and of a possible heterogeneity of zeolite sites acting as anions. In summary, the set of IR data allows inferring that 1,5-hexadiene molecules in *HS-MOR* participate in carbocation-based reactions that, on the basis of the 80% decrease in intensity of the $\nu(\text{C}=\text{C})$ signal (1641 cm^{-1}), involve the large majority of monomers.

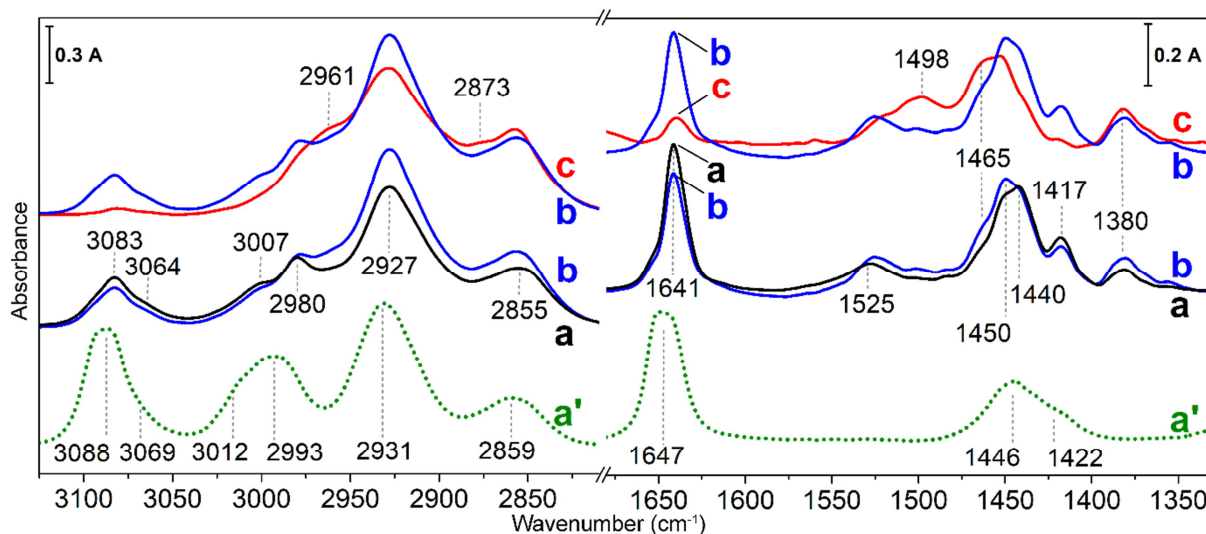


Figure 4. IR spectra of 1,5-hexadiene: a') in vapor phase, at $p=25$ mbar; a) immediately after contact with *HS-MOR* (pre-outgassed at r.t. for 1 h), at $p=50$ mbar; b) after 1h of contact; c) after 1 week of contact, and outgassing at r.t. for 1 h. Spectra a-c are reported as resulting from the subtraction of the spectrum of *HS-MOR* prior 1,5-hexadiene adsorption. Spectrum b is shown in duplicate, for the sake of comparison with spectrum c.

Table 2. Assignment of 1,5-hexadiene infrared absorptions.

mode	Frequency (cm^{-1})		
	gas phase ($p=10$ mbar)	<i>HS-MOR hexa</i> (immediately after adsorption)	<i>HS-MOR hexa</i> (new signals rising during time evolution)
$\nu_{\text{as}}\text{CH}_2$ (sp^2)	3088	3083	3080
$\nu\text{C}=\text{C} + \delta_{\text{ip}}\text{CH}_2$ (sp^2) ^[1]	3069	3066	
νCH (sp^2)	3012	3007	
$\nu_{\text{s}}\text{CH}_2$ (sp^2)	2993	2980	
$\nu_{\text{as}}\text{CH}_3$			2961
$\nu_{\text{as}}\text{CH}_2$ (sp^3)	2931	2927	
$\nu_{\text{s}}\text{CH}_3$			2873
$\nu_{\text{s}}\text{CH}_2$ (sp^3)	2859	2855	
$\nu\text{C}=\text{C}$	1647	1641	
$\delta_{\text{as}}\text{CH}_3$			1465
δCH_2 (sp^3)	(unresolved) 1446	1450	
δCH_2 (sp^3)	(unresolved) 1446	1440	
$\delta_{\text{ip}}\text{CH}_2$ (sp^2)	1422	1417	
$\delta_{\text{s}}\text{CH}_3$			1380

as: antisymmetric; s: symmetric; ip: in plane

[*] From ref.^[88] The other assignments are from ref.^[87]

1,5-hexadiene in *HS-MOR*: quantitative aspects

To gather a quantitative estimation of the guest species contained in the zeolite porosities, we performed thermal analyses on the sample after completion of the reactive processes, using as a reference the unloaded zeolite. Figure 5 shows the thermal gravimetric analysis (TGA) and the corresponding differential thermogravimetry curve of *HS-MOR* and of *HS-MOR hexa* after one week of reaction (i.e. sample in spectrum c in Figure 4). When loaded in the TGA cell, both samples were exposed to air. Below 200 °C, the unloaded *HS-MOR* (curves a and a') shows a first weight loss (1.9 wt.%) in two distinguishable steps accounting for superficial water and water loosely adsorbed within the channels. A second weight loss of 2 wt.% occurs in the 400 - 800 °C range, in good agreement with the silanol condensation process discussed by Fantini et al.^[82]

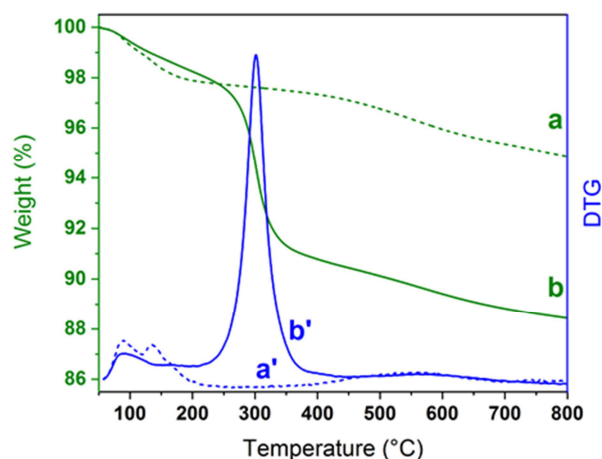


Figure 5. TG (green) and DTG curves (blue) for of *HS-MOR* (a, a') and *HS-MOR hexa* (b, b').

The *HS-MOR hexa* (curves b and b') sample shows a reduced weight loss of 1.5 wt.% below 200 °C which can be justified by a lesser quantity of water molecules within the zeolite channels, likely due to the presence of co-hosted *hexa* molecules. Confirmatory evidence of the decrease in water content of *HS-MOR hexa* was provided by XRPD data analysis (*vide infra*). The main weight loss of 7.5 wt.% occurs in the 200–450 °C range, suggesting a unique process for the release of all the organic moieties. Above 450 °C, also in this sample, a further weight loss of 1.8 wt.% due to the condensation of silanols is observed. As a whole, considering the number of hydroxyls in the *HS-MOR* to be constant before and after the *hexa* loading, the weight loss due to organic moieties corresponds to the presence, on an average, of ca. 2.9 *hexa* molecules per unit cell, i.e. ca. 1.5 molecules per each of the two 12 MR channels in a unit cell. Thus, the reaction evidenced by IR spectroscopy not only involved most of the 1,5-hexadiene molecules, but it also took place within the majority of the zeolite porosity, as also further substantiated by the structural analysis.

1,5-hexadiene in *HS-MOR*: experimental structural aspects

From the XRPD patterns reported in Figure 6, it is possible to observe differences in the relative intensities of low angle peaks of *HS-MOR* and *HS-MOR hexa* samples. This is a clear indication of the penetration of 1,5-hexadiene molecules in the zeolite pores, partially occupied by only H₂O molecules in the pristine sample, as found in the case of phenylacetylene.^[55]

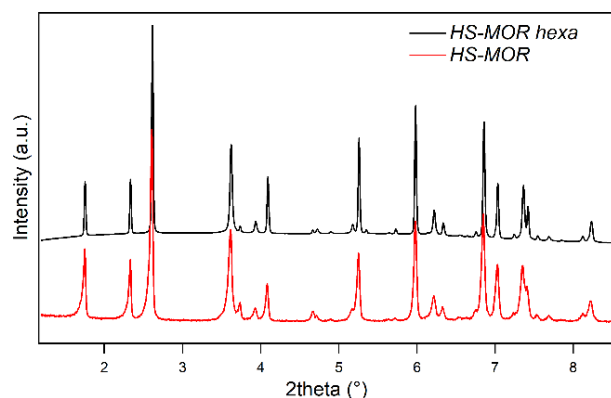


Figure 6. Comparison of the XRPD patterns of *HS-MOR*^[81] and *HS-MOR hexa*. The two patterns have been rescaled and normalized for the same intensity on the third peak, at 2.6°. Selected 2 theta range is reported (full patterns are reported in Figure 3S in the Supporting Information).

Upon the inspection of the difference Fourier map, it was possible to locate a chain composed by six carbon atoms in the 12MR channel, as reported in Figure 7, that lies on the plane perpendicular to [100]. The carbon atoms forming the chain occupy two crystallographic positions C₁ and C₂ (with an average C-C distance ~ 1.5 Å) accounting for 2 and 4 carbon atoms in each channel of the unit cell, respectively. As a whole, based on the C sites multiplicity and on their full occupation, twelve C atoms are hosted in each unit cell - that is, one six membered chain per channel (i.e. two six membered chain p.u.c.) whose axis coincides with the [001] direction. Noteworthy, residual maxima are present in the Fourier map located around the chain (Figure 7b-c),

suggesting that side moieties could be present in the side pockets as well, in a disordered arrangement.

This observation provides evidence that sub-sets of the six membered C atoms chain should derive from different 1,5-hexadiene molecules. The average distance of ~1.5 Å between C-C atoms (see Table S2) indicates the formation of a continuous C atom chain running along the 12MR channel (Figure 7a).

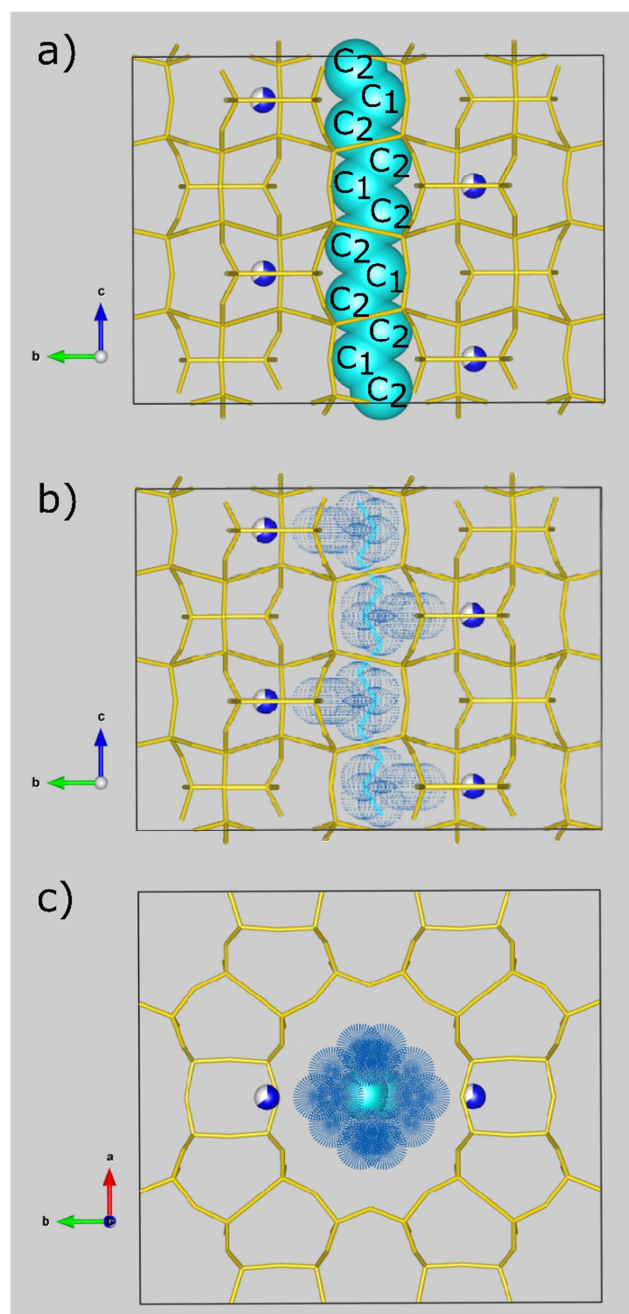


Figure 7. Details of *HS-MOR hexa* structure, data obtained by XRPD structural refinement. Water molecules are represented in blue, while carbon atoms are in cyan. For clarity, just the extraframework content occupying the central channel is reported. a) *HS-MOR hexa* structure reported along [100] direction b) *HS-MOR hexa* structure reported along [100] direction showing the residual maxima (blue clouds) of the Fourier map positioned around the C₁-C₂ chain (in cyan) c) *HS-MOR hexa* structure reported along [001] direction showing the residual maxima (blue clouds) of the Fourier map positioned around the C₁-C₂ chain (in cyan).

The full occupancy of all the carbon sites indicates an extended polymerization reaction of the 1,5-hexadiene molecules into the channels, in agreement with the IR results. It is worth noting that, since the de-alumination procedure - aimed at the obtainment of a high silica phase - induces strong defectivity, the starting zeolite presents a certain degree of mesopores and defects.^[55] We can assume that the detected chain occupies basically the ordered microporous volume of the sample. An additional peak of the difference Fourier map was ascribed to a H₂O molecule site in the window between the 12MR and the side pocket, corresponding to the W₁ site found in the pristine sample.^[81] The refinement of the occupancy factor leads to a total H₂O amount of 3.5 molecules per unit cell. This is in agreement with the results of the thermal analysis, indicating a water content of about 2.6 molecules per unit cell (corresponding to 1.5 wt%). The water present in the channel is re-adsorbed once the sample is recovered in air after the 1,5-hexadiene loading. After 1,5-hexadiene reaction, the cell parameters of the loaded sample show only a slight increase, mainly related to the lengthening of the *b* parameter. In fact, once the *hexa* molecules are hosted in the zeolite pores, the channels adapt to the new host: the 12MR channel becomes more circular and, as a consequence, the 8MR channel further lengthens along *a* direction. The lengthening of the *b* parameter is mainly due to the rotation of the Si₃ and Si₄ tetrahedra belonging to the 4MR ring (Table 3 and Figure 8).

This mechanism induces the lengthening of the O₉-O₁₀ distance, oriented along *b*. Conversely, the O₁₀-O₁₀ diameter of the 12MR channel remains almost unchanged, due to the steric hindrance of the organic chain lying on the *bc* plane. The polymer chain weakly interacts with the framework oxygen O₁₀, as suggested by the C₂-O₁₀ distance equal to about 3.6 Å (Table 2S, Supporting Information).

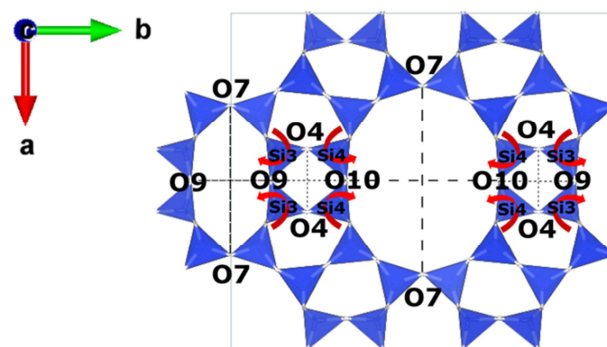


Figure 8. Mechanism of cell adapting due to the polymer formation: the 12MR channel becomes more circular and, as a consequence, the 8MR channel further lengthens along *a* direction.

Table 3. 12MR and 8MR channel diameters and angles of *HS-MOR*^[81] and *HS-MOR hexa*. The ellipticity parameters *E* is defined as the ratio between the largest and the smallest O-O diameters, the Crystallographic Free Area (CFA) is also reported.

	<i>HS-MOR</i> ^[a]	<i>HS-MOR hexa</i> ^[b]
12MR		
O ₇ -O ₇	10.02	9.81(3)
O ₁₀ -O ₁₀	8.85	8.86(5)
<i>E</i>	1.13	1.11
CFA (Å ²)	35.1	
8MR		
O ₇ -O ₇	8.03	8.25(3)
O ₉ -O ₉	5.58	5.52(4)
<i>E</i>	1.44	1.5
CFA (Å ²)	10.61	
4MR		
O ₉ -O ₁₀	4.01	4.06(3)
O ₄ -O ₄	3.35	3.33(3)
O ₄ -O ₁₀ -O ₄	77.82	77.029(2)
O ₉ -O ₄ -O ₁₀	100.28	100.808(2)

[a] From Ref.^[81]. [b] This work.

Modeling of 1,5-hexadiene reacted in *HS-MOR*

The features emerging from the above-presented spectroscopic, thermogravimetric and structural data could only provide an average picture of the composite system. A microscopic insight required the following computational analyses. Figure 9 depicts the optimized structures of the five different model polymers considered in our study, presented at the beginning of this Section, and now located within the zeolite 12 MR channels. They constitute a representative sample of the possible ways in which 1,5-hexadiene molecular units could be assembled into a continuous 1-D structure incorporated in *HS-MOR*.

It is apparent that all model polymers are compatible with the geometric restrictions of the zeolite channels. Most importantly, calculations indicate that they are all stabilized by the zeolite framework. Specifically, the *HS-MOR*/polymer binding energies are -29.65, -41.64, -43.60, -40.07, -38.80 kcal mol⁻¹ per simulation cell (p.s.c.) for Models A, B, C, D, E, respectively.

Such an ordering of the binding energies can be understood by considering the nature of the dominant host-guest interactions.

The composition of the polymers and the *HS-MOR* framework indicates that the host-guest interactions in these composites should be essentially of the van der-Waals type. Accordingly, the model having, by far, the smallest binding energy is Model A - which contains the simple 1,5-hexadiene derived polymer without side moieties (poly(methylene)), eventually resulting from a head-tail reaction for all molecules. The stabilizing effect of the zeolite framework is lowest for this composite because Model A exhibits the largest separation between the polymer chain and the zeolite walls (minimum C-O_{framework} distance = 3.85 Å).

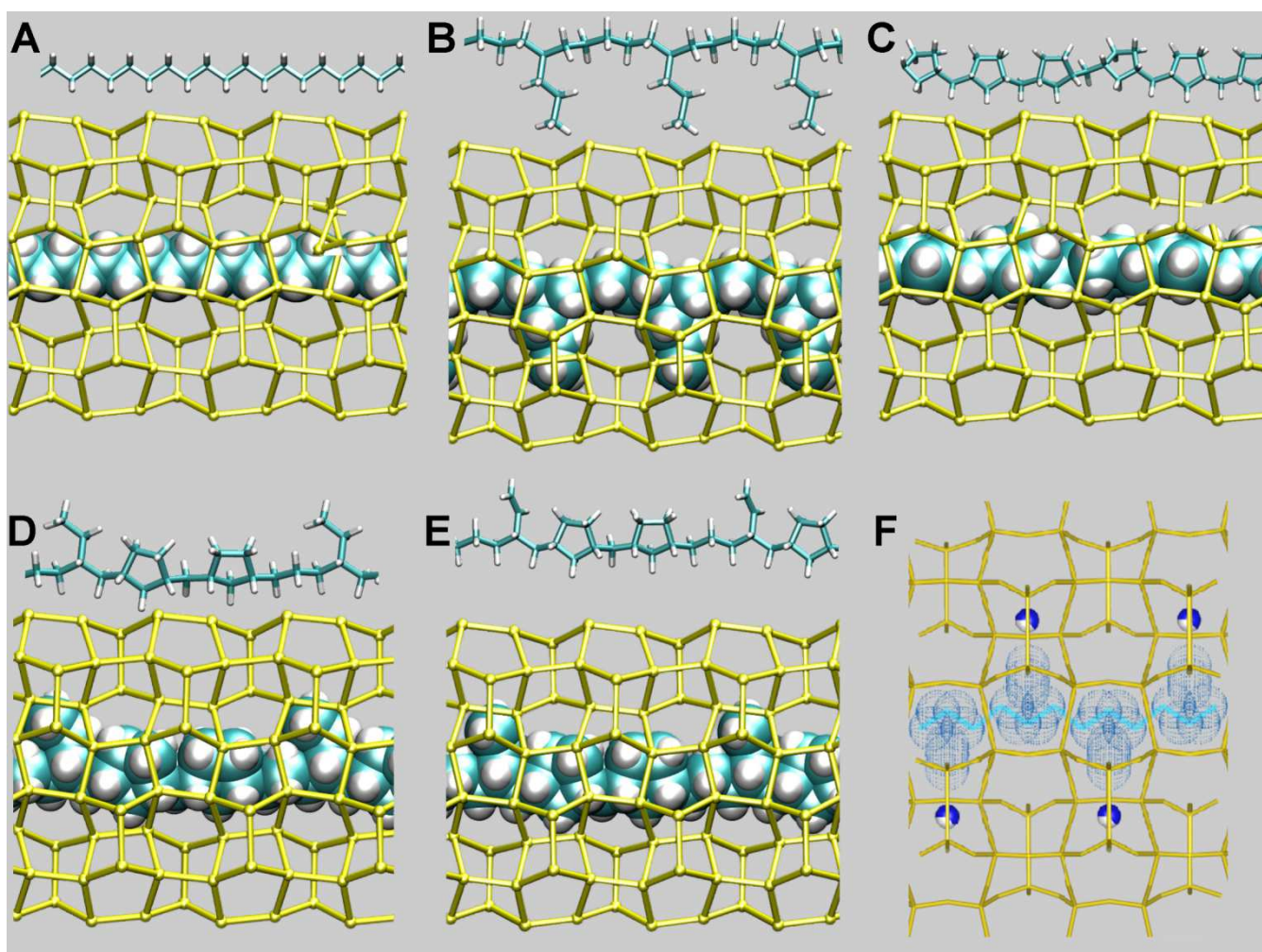


Figure 9. A-E): Graphical representation of the optimized structures of *HS-MOR* encapsulating: Model A) linear, non-branched alkyl polymer chain; Model B) chain with side propyl groups penetrating in the MOR side pockets; Model C) all-cyclopentane-chain featuring a PMCP polymer; Model D) chain containing two cyclopentane units and one branching ethyl group p.s.c.; Model E) chain containing two cyclopentane units and one branching vinyl group p.s.c.. The five 1,5-hexadiene based polymer chains inside the *HS-MOR* framework are highlighted in van-der-Waals representation. For each model composite, the correspondent polymer chain is also shown on top of the composite in stick representation. All the five polymer chains are stabilized by the *HS-MOR* framework. Color codes: *HS-MOR* framework=yellow; C=cyan; H=white. F): *HS-MOR* hexa structure showing the residual maxima of the Fourier map positioned around the C1-C2 chain (color codes as in Figure 7b). All structures are projected in the bc plane.

In contrast, the minimum $C-O_{\text{framework}}$ distances exhibited by the other models are considerably shorter (3.18 Å, 3.31 Å, 3.24 Å, and 3.28 Å for Models B, C, D, E, respectively) and well in line with the values found for other bulky organic species encapsulated in zeolite channels.^[28,31,89–94]

Hence, Model A could be considered as the least probable structure among the five models. This hypothesis is also in line with the IR data, which evidenced an appreciable proportion of terminal methyl groups. Indeed, Model B – which features side propyl groups hosted in the *HS-MOR* side pockets – is considerably more favorable as its binding energy p.s.c. is about 12 Kcal mol⁻¹ greater than Model A.

Among the five models, Model B exhibits the shortest minimum $C-O_{\text{frame}}$ distance (3.18 Å), which is related to the partial penetration of the propyl side chain in the MOR side pockets (Figure 9b). Model C contains a 1-D chain of cyclopentane units, known as poly(methylene-1,3 cyclopentane). This polymer was identified as a maximum-order product of the polymerization of

1,5-hexadiene in presence of homogeneous Ziegler-Natta catalysts.^[70,95,96] In our case, Model C exhibits the greatest binding energy among the five models, likely because of the optimal host-guest contacts inside the *HS-MOR* main channels. The 1-D cyclopentane chain perfectly fits into the 12MR void space, so maximizing the favorable van-der-Waals interactions with the host without inducing significant distortion of the *HS-MOR* framework.

On the other hand, the IR evidence of terminal methyl groups suggests that the ideal polycyclopentane chain in Model C should be less likely than a branched polymer. Hence Model D – which features both branching alkyl groups and cyclopentane units – might be a more realistic model of the polymer chain inside MOR: its binding energy is comparable to Models B and C, and the ethyl branching group can be well accommodated inside the main channel of the host. Finally, Model E contains a branching vinyl group, and it is structurally and energetically very close to Model D.

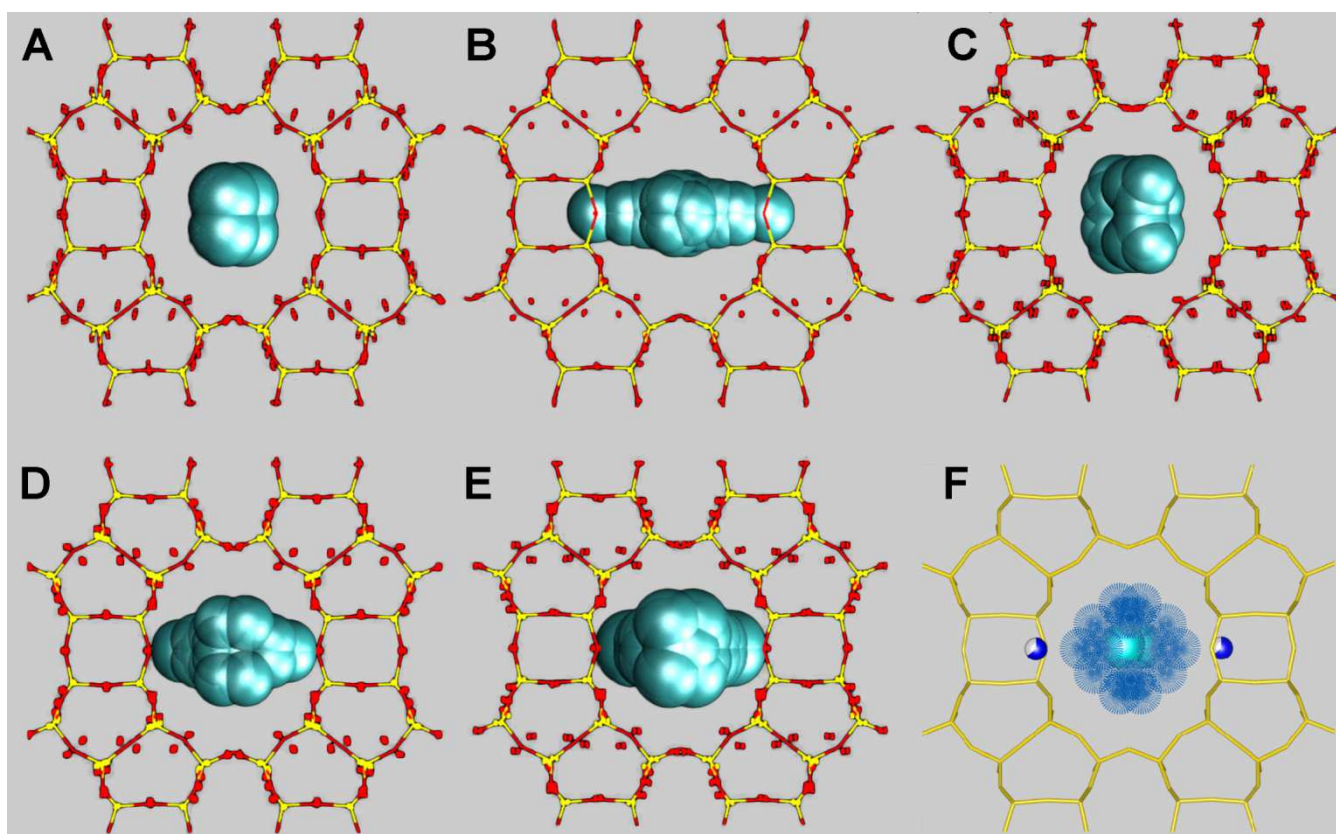


Figure 10. A-E): Symmetrized optimized structures of Models A-E projected in the *ab* plane (Si, O = dots; C= van der Waals spheres) superposed on the XRPD structure of the framework (represented as sticks). The symmetrized optimized structures were obtained by applying the symmetry operations of the *Cmcm* space group of *HS-MOR* to the optimized atomic positions of each model. Color codes: Si=yellow; O=red; C=cyan. F): XRPD structure of *HS-MOR* hexa also showing the residual maxima of the Fourier map positioned around the C₁-C₂ chain (color codes as in Figure 7c).

Since the IR analyses indicate that the almost complete loss of the double C=C bonds signals occurs over a very long time (about a week), Model E might actually represent a possible model for the 1-D chain which still contains some unreacted double bonds.

A visual comparison of Models A-E with panel F in Figure 9 suggests that some of these models might be representative of the refined structure. To establish which of the five models better compares with the XRPD data, we superposed the symmetrized structure of each model to the refined structure.

To perform the comparison, we applied to the calculated atomic positions of our models the symmetry operations of the *Cmcm* group. As well known, the refined structure of the composite actually results from averaging over a number of different configurations characterized by a symmetry lower than that of the ideal zeolite framework.^[42] Indeed, figures 10a-e clearly show that the computed positions of the framework atoms are symmetrically distributed around the lines denoting the refined structure. In line with results obtained on other zeolite frameworks,^[42,97,98] the “averaging effect” is especially evident for the O positions due to the inherent flexibility of the Si-O-Si angles. Overall, such a comparison underlines quite a good agreement between calculated and refined framework structures. Focusing now on the polymer structure, a closer inspection of Figure 10 reveals that the two models containing both cyclopentyl units and side moieties (Models D, E) best match the experimental results. On the other hand, the simple linear C-C

chain of Model A exhibits the worst comparison with the residual maxima of the Fourier map, because of its low steric encumbrance. Indeed, all the other model polymers – which are all bulkier than the simple linear chain – better fit to the *HS-MOR* main channel, as indicated by the closer C-O_{framework} contacts and evidenced in Figure 10b-e.

Interestingly, Model B features two carbon symmetrized positions – those corresponding to the terminal methyl group of the propyl branching chain- located in the window between the 12MR and the side pocket. Therefore, these locations that were ascribed to a H₂O molecule site (W₁) in the XRPD refinement – might also be due to terminal methyl groups of propyl side moieties. However, with respect to the cyclopentyl-containing chains in Models C, D, E, the polymer in Model B would require a higher number of (formal) H₂ molecules to saturate the double bond (two per diene molecules). Hence, on the basis of the comparison of the computational models with the XRPD and spectroscopic data, we propose that the most probable structure of the caged 1,5-hexadiene derived polymer might be similar to Model D – i.e. a 1D-polymer featuring both cyclopentane units and side alkyl moieties. The formation of polymers containing vinyltetramethylene (VTM) units from 1,5-hexadiene, which may undergo subsequent functionalization, has been documented to occur with homogeneous Ziegler-Natta catalysts.^[70,99] Keeping into account the long time scale of the full process as deduced by IR measurements (one week), model E - featuring vinyl side groups

between cyclic units – might be a plausible representation of a possible first product of the polymerization, which could probably proceed via both insertion-cyclizations and successive 1,2 insertions of 1,5-hexadiene units.

Conclusion

In this work we adopted a multidisciplinary approach to study the fate of a flexible guest α,ω -diene molecule (1,5-hexadiene) hosted in the channels of a moderately acid zeolite. Such a molecule is known to produce different moieties and even oligomers or polymers in homogeneous media, whose chain length and microstructure is very sensitive to the catalyst structure and to the adopted conditions. Here we showed that, in confining hydrophobic nanochannels at ambient conditions, the guest molecules undergo a slow transformation to a continuous polymeric chain, consisting of cyclic units intercalated by short side chains, that nicely fits to the host channels. Importantly, despite the appearance of olefinic side groups along the main chain in the course of the process, cross linking is prevented by the confining environment of the zeolite channel, which forces a linear growth of the polymer. Hence, our work evidences the relevance of the size-shape geometrical constraints of zeolite channels to drive organization at molecular level. Thanks to the presence of few acid sites evenly distributed along the channel walls, once the molecules are properly organized inside the void-space architecture, they are prone to react yielding quasi monodimensional polymers, whose structure is shaped by the geometrical features of the zeolite mold. In addition, the IR monitoring has shown that the silanols of *HS-MOR* are strong enough to protonate an adsorbed electron-donor probe. This kind of reactivity, not often observed for high-silica zeolites, accounts for the formation of observed carbocations and for the polymerisation of 1,5-hexadiene in very mild conditions of temperature and concentration. The next challenge would be to achieve further control of the microstructure and stereochemistry of the confined polymer. This goal could be accomplished by integrated experimental and theoretical investigations of this intriguing phenomenon aimed at understanding its delicate mechanistic aspects, for example by varying the reaction conditions of the shape-directed polymerization process. Beside opening fascinating questions on the inner machinery of confined polymerization, our results underline that zeolite frameworks are also effective in directing covalent bonds' cleavage-formation events at room conditions, leading to arrays of polymers, each shaped by the zeolite mold. This awareness may further encourage the production of encapsulated arrays of low-dimensionality organic polymeric nanostructures with potential application in a variety of end uses.

Experimental Section

Materials

High-silica mordenite (*HS-MOR*, $\text{SiO}_2/\text{Al}_2\text{O}_3$ ratio ~ 200; $\text{Na}_2\text{O} < 0.1$ wt.%) was purchased from the Tosoh Corporation (Japan) in its protonated form (code HSZ-690HOA). 1,5-hexadiene (abbreviated *hexa*, C_6H_{10}) was purchased from Sigma-Aldrich (97% purity).

High-silica mordenite loading

The loading of 1,5-hexadiene was performed on a previously outgassed *HS-MOR* at room temperature (r.t.) for 1 h, in order to remove physisorbed water, by contacting the zeolite powder with 50 mbar of 1,5-hexadiene vapor for an increasing amount of time up to one week at r.t. followed by *in situ* IR spectroscopy. Samples were then outgassed (1 h, r.t.) and exposed to air before thermogravimetric and X-ray Powder Diffraction (XRPD) measurements. The loaded sample are labelled *HS-MOR hexa*.

Thermogravimetric analysis

TG analyses of pure *HS-MOR* and of *HS-MOR hexa* were carried out using an SDT Q600 thermal analyzer from TA Instruments by an initial fluxing of the sample under nitrogen for 60 min at 50 °C in the sample chamber to remove environmental fluctuations, then by increasing the temperature from 50 up to 800°C with a ramp of 10°C/min under synthetic air flow.

IR experiments

Absorption IR spectra were collected at r.t. with a Perkin-Elmer FT-IR System 2000 spectrophotometer equipped with an MCT detector, working in the range of wavenumbers 7200–580 cm^{-1} at a resolution of 2 cm^{-1} (number of scans 64). For IR analysis the powder of *HS-MOR* was compressed in self-supporting discs, with an optical thickness of about 10 mg cm^{-2} , placed in a home-made quartz IR cell equipped with KBr windows and connected to a glass vacuum line (residual pressure: 1×10^{-4} mbar), allowing *in situ* adsorption and desorption experiments to be carried out. The spectrum of 1,5-hexadiene in the vapor phase was collected introducing the vapors of the molecule at $p = 25$ mbar in a cell for gas measurements, with an optical path of 10 cm.

XRPD experiments

X-ray powder diffraction experiment was performed at ID15b beamline of ESRF (Grenoble) on the 1,5-hexadiene-loaded samples (*HS-MOR hexa*). The powder was placed in a 0.3 mm quartz capillary mounted on a goniometric spinning head. The diffraction data ($\lambda = 0.412015$ Å) were collected in the Debye–Scherrer geometry on a MAR555 detector with a sample-distance of 547.5 mm. A one-dimensional diffraction pattern was obtained by integrating the two-dimensional images with the program Dioptas^[100]. A preliminary data collection of *HS-MOR hexa* was performed at ID22 beamline at ESRF.

Rietveld profile fitting was performed in the *Cmcm* space group using the GSAS package^[101] with the EXPGUI^[102] interface, starting from the framework atomic coordinates reported in^[101]. The extra-framework sites (water and organic moieties) were localized from the difference Fourier map. The background curve was fitted using a Chebyshev polynomial with 28 coefficients. The pseudo-Voigt profile function proposed by Thompson and coauthors^[103] was used with a peak intensity cut-off set to 0.1% of the strongest peak. Soft-restraints were applied to the T–O distances (1.60 Å) and C–C distances (1.5 Å), their weight was set at 1000. The isotropic displacement parameters were constrained in the following way: a value for all the tetrahedral cations (Si), a second value for all the framework oxygen atoms, a third value for the carbon atoms and a fourth one for H_2O molecules.

Theoretical Calculations

Our computational models for *HS-MOR hexa* contain two MOR crystallographic unit cells along the *c* direction. The total volume of the simulation cell was $a \times b \times 2c$, where the *a*, *b*, and *c* parameters were the ones experimentally determined for *HS-MOR hexa*. Due to the very low density of Brønsted acid sites experimentally detected with respect to the simulation cell size (less than one acid site per simulation cell), the host was modeled as an all-silica MOR framework with stoichiometry $[\text{Si}_{196}\text{O}_{192}]$

per simulation cell (p.s.c.). This framework model was then filled with putative models of continuous 1-D polymers that might be formed upon polymerization of 1,5-hexadiene moieties. In particular, we considered five models of 1,5-hexadiene based polymers (depicted in figure 2), labelled as A, B, C, D, E and with stoichiometry p.s.c. equal to $C_{12}H_{24}$, $C_{18}H_{36}$, $C_{18}H_{30}$, $C_{18}H_{32}$, and $C_{18}H_{30}$, respectively. Only one channel of the framework was filled with polymer models. All the above-mentioned model systems were simulated using a Density-Functional-Theory (DFT) computational approach. As DFT approximation, we used PBE with dispersion corrections.^[104] Although the DFT machinery surely has limitations due to self-interactions^[105,106] for most purposes such scheme delivers a satisfactory accuracy- at a viable cost, as evidenced by benchmark calculations on various zeolitic frameworks.^[107-112] The selection of PBE-D2 for the present case was prompted by its reliability in reproducing the average framework structure of LTL,^[113] high-silica ferrierite,^[42,98] and chabazite^[97] obtained from *in situ* diffraction experiments. Such protocol delivers an adequate description of physico-chemical properties of molecules at material interfaces.^[114-119] The computational cell was large enough to perform gamma-point only calculations.^[120] The guess for the various models were built using the optimized geometry of this framework (simulation cell stoichiometry = $[Si_{96}O_{192}]$) as a starting point. Prior to geometry optimization, all models were annealed by means of ab initio molecular dynamics (AIMD)^[120,121] trajectories. Our selected time step was 0.121 fs, the inertia parameter for the electronic coefficients was 500 a.u. The plane-wave-basis set size was determined by the wavefunction cutoff (25 Ry) and density cutoff (200 Ry). The selected theoretical methodology treats the interactions of electrons with the ionic cores by means of pseudopotentials: of the ultrasoft type^[122] for O, C, H, and norm conserving with non-linear core corrections^[123] for Si. Importantly, no symmetry constraints were imposed to the atomic positions during the calculations, only the simulation cell parameters (with periodic boundary conditions) were kept fixed at the experimental values. Our convergence criterion for geometry optimizations required a maximum force on the ions below 1×10^{-4} Hartree/Bohr.^[120] Minimum energy structures were obtained by optimization of the above mentioned models using different initial guess configurations. The different number of atoms composing the polymers prevents a direct comparison of their formation energies. For each of these five systems, the lowest energy geometry was selected to evaluate the binding energy of the polymer chain inside HS-MOR. Binding energies were evaluated with the following equation:

$$\Delta E(HS-MOR \text{ hexa}) = E(HS-MOR \text{ hexa}) - E(HS-MOR) - E(\text{hexa})$$

Where ΔE is the binding energy of the composite, while $E(HS-MOR \text{ hexa})$, $E(HS-MOR)$, $E(\text{hexa})$ represent the total energy of the composite, of the empty HS-MOR, and of the hexa based polymeric chain, respectively, all calculated in the same simulation cell. Negative values of the binding energy denote a favorable interaction of the polymer with HS-MOR. Binding energies reported in the text are expressed in kcal per mol of simulation cell. The CPMD code^[124] was used for all calculations. The computed structures were visualized with the VMD and Avogadro codes.^[125]

Acknowledgements

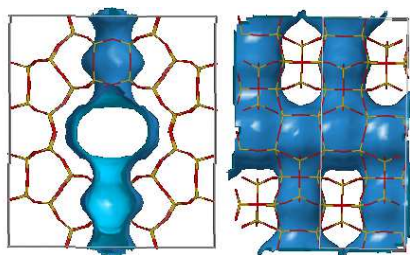
This work was carried out in the framework of the PRIN project ZAPPING (PRIN2015 Prot.2015HK93L7) funded by the Italian MIUR. FAR2018 Uninsubria is acknowledged for funding. M. Fabbiani is gratefully indebted to C. Nannuzzi for the support in the *in situ* experiments and data elaborations. Authors thank the staff of ID15b and ID22, ESRF, for the help in X-ray diffraction data collection.

Keywords: zeolites • polymerization • nanostructures • density functional calculations • infrared spectroscopy • X-Ray Diffraction

- [1] U. Diaz, A. Corma, *Chem. - A Eur. J.* **2018**, *24*, 3944–3958.
- [2] G. Calzaferri, S. Huber, H. Maas, C. Minkowski, *Angew. Chemie - Int. Ed.* **2003**, *42*, 3732–3758.
- [3] H. Garcia, V. I. Parvulescu, *Catal. Sci. Technol.* **2018**, *8*, 4834–4857.
- [4] E. M. Gallego, C. Li, C. Paris, N. Martin, J. Martinez-Triguero, M. Boronat, M. Moliner, A. Corma, *Chem. - A Eur. J.* **2018**, *24*, 14631–14635.
- [5] F. Cucinotta, A. Guenet, C. Bizzarri, W. Mroz, C. Botta, B. Milian-Medina, J. Gierschner, L. De Cola, *Chempluschem* **2014**, *79*, 45–57.
- [6] A. Corma, H. Garcia, *Eur. J. Inorg. Chem.* **2004**, *2004*, 1143–1164.
- [7] D. Balestri, P. P. Mazzeo, C. Carraro, N. Demitri, P. Pelagatti, A. Bacchi, *Angew. Chemie Int. Ed.* **2019**, *58*, 17342–17350.
- [8] G. Campillo-Alvarado, M. M. D'mello, M. A. Sinnwell, H. Höpfl, H. Morales-Rojas, L. R. MacGillivray, *Front. Chem.* **2019**, *7*, 695.
- [9] G. L. Hill, E. Bailey, M. C. Stennett, N. C. Hyatt, E. M. Maddrell, P. F. McMillan, J. A. Hriljac, *J. Am. Chem. Soc.* **2011**, *133*, 13883–13885.
- [10] P. Lu, L. Gómez-Hortigüela, M. A. Cambor, *Chem. - A Eur. J.* **2019**, *25*, 1561–1572.
- [11] G. Tabacchi, *ChemPhysChem* **2018**, *19*, 1249–1297.
- [12] J. Čejka, A. Corma, S. Zones, *Zeolites and Catalysis: Synthesis, Reactions and Applications, Volume 2*, WILEY-VCH Verlag GmbH & Co. KGaA, Weinheim, Germany, **2010**.
- [13] E. Fois, G. Tabacchi, S. Quartieri, G. Vezzalini, *J. Chem. Phys.* **1999**, *111*, 355–359.
- [14] S. Quartieri, A. Sani, G. Vezzalini, E. Galli, E. Fois, A. Gamba, et al., *Microporous Mesoporous Mater.* **1999**, *30*, 77–87.
- [15] E. Fois, A. Gamba, C. Medici, G. Tabacchi, S. Quartieri, E. Mazzucato, R. Arletti, G. Vezzalini, V. Dmitriev, *Microporous Mesoporous Mater.* **2008**, *115*, 267–280.
- [16] A. R. Morgado Prates, F. Meunier, M. Dodin, R. Martinez Franco, D. Farrusseng, A. Tuel, *Chem. - A Eur. J.* **2019**, *25*, 2972–2977.
- [17] R. Bueno-Perez, S. R. G. Balestra, M. A. Cambor, J. G. Min, S. B. Hong, P. J. Merkl, S. Calero, *Chem. - A Eur. J.* **2018**, *24*, 4121–4132.
- [18] L. R. Aramburo, L. Karwacki, P. Cubillas, S. Asahina, D. A. M. De Winter, M. R. Drury, I. L. C. Buurmans, E. Stavitski, D. Mores, M. Daturi, et al., *Chem. - A Eur. J.* **2011**, *17*, 13773–13781.
- [19] A. M. Pintus, A. Gabrieli, F. G. Pazzona, G. Pireddu, P. Demontis, *Phys. Chem. Chem. Phys.* **2019**, *21*, 7879–7884.
- [20] H. I. Hamoud, M. Lafjah, F. Douma, O. I. Lebedev, F. Djafri, V. Valchev, M. Daturi, M. El-Roz, *Sol. Energy* **2019**, *189*, 244–253.
- [21] D. Comboni, F. Pagliaro, P. Lotti, G. D. Gatta, M. Merlini, S. Milani, M. Migliori, G. Giordano, E. Catizzone, I. E. Collings, et al., *Catal. Today* **2020**, *345*, 88–96.
- [22] J. Džedeček, Z. Sobalík, B. Wichterlová, *Catal. Rev. - Sci. Eng.* **2012**, *54*, 135–223.
- [23] F. C. Hendriks, J. E. Schmidt, J. A. Rombouts, K. Lammertsma, P. C. A. Bruijninx, B. M. Weckhuysen, *Chem. - A Eur. J.* **2017**, *23*, 6305–6314.
- [24] M. Zaarour, H. El Siblani, N. Arnault, P. Boullay, S. Mintova, *Materials (Basel)*. **2019**, *12*, 2830.
- [25] P. Cao, O. Khorev, A. Devaux, L. Sägesser, A. Kunzmann, A. Ecker, R. Häner, D. Brühwiler, G. Calzaferri, P. Belsler, *Chem. - A Eur. J.* **2016**, *22*, 4046–4060.
- [26] I. López-Duarte, Le-Quyenha Dieu, I. Dolamic, M. V. Martínez-Díaz, T. Torres, G. Calzaferri, D. Brühwiler, *Chem. - A Eur. J.* **2011**, *17*, 1855–1862.
- [27] X. Zhou, T. A. Wesolowski, G. Tabacchi, E. Fois, G. Calzaferri, A. Devaux, *Phys. Chem. Chem. Phys.* **2013**, *15*, 159–167.
- [28] H. Manzano, L. Gartzia-Rivero, J. Bañuelos, I. López-Arbeloa, *J. Phys. Chem. C* **2013**, *117*, 13331–13336.
- [29] G. Tabacchi, E. Fois, G. Calzaferri, *Angew. Chemie Int. Ed.* **2015**, *54*, 1112–1116.
- [30] G. Calzaferri, H. Li, D. Brühwiler, *Chem. - A Eur. J.* **2008**, *14*, 7442.
- [31] L. Gigli, R. Arletti, G. Tabacchi, M. Fabbiani, J. G. Vitillo, G. Martra, A. Devaux, I. Miletto, S. Quartieri, G. Calzaferri, et al., *J. Phys. Chem. C* **2018**, *122*, 3401–3418.
- [32] P. Woodtli, S. Giger, P. Müller, L. Sägesser, N. Zucchetto, M. J. Reber, A. Ecker, D. Brühwiler, *Dye. Pigment.* **2018**, *149*, 456–461.
- [33] R. Sola-Llano, V. Martínez-Martínez, Y. Fujita, L. Gómez-Hortigüela, A. Alfayate, H. Uji-i, E. Fron, J. Pérez-Pariente, I. López-Arbeloa, *Chem. - A Eur. J.* **2016**, *22*, 15700–15711.
- [34] A. Bertucci, H. Lülff, D. Septiadi, A. Manicardi, R. Corradini, L. De Cola, *Adv. Healthc. Mater.* **2014**, *3*, 1812–1817.
- [35] L. Giussani, G. Tabacchi, S. Coluccia, E. Fois, *Int. J. Mol. Sci.* **2019**, *20*, 2965.
- [36] F. Cucinotta, F. Carniato, A. Devaux, L. De Cola, L. Marchese, *Chem. - A Eur. J.* **2012**, *18*, 15310–15315.
- [37] G. Tabacchi, E. Gianotti, E. Fois, G. Martra, L. Marchese, S. Coluccia, A. Gamba, *J. Phys. Chem. C* **2007**, *111*, 4946–4955.

- [38] L. Grösch, Y. J. Lee, F. Hoffmann, M. Fröba, *Chem. - A Eur. J.* **2015**, *21*, 331–346.
- [39] E. Fois, A. Gamba, G. Tabacchi, S. Coluccia, G. Martra, *J. Phys. Chem. B* **2003**, *107*, 10767–10772.
- [40] A. J. Bagnall, M. Santana Vega, J. Martinelli, K. Djanashvili, F. Cucinotta, *Chem. - A Eur. J.* **2018**, *24*, 11992–11999.
- [41] A. J. Sindt, M. D. Smith, S. Berens, S. Vasenkov, C. R. Bowers, L. S. Shimizu, *Chem. Commun.* **2019**, *55*, 5619–5622.
- [42] R. Arletti, E. Fois, L. Gigli, G. Vezzalini, S. Quartieri, G. Tabacchi, *Angew. Chemie - Int. Ed.* **2017**, *56*, 2105–2109.
- [43] G. D. Gatta, P. Lotti, G. Tabacchi, *Phys. Chem. Miner.* **2018**, *45*, 115–138.
- [44] L. Gigli, R. Arletti, E. Fois, G. Tabacchi, S. Quartieri, V. Dmitriev, G. Vezzalini, *Crystals* **2018**, *8*, 79.
- [45] D. J. Cardin, *Adv. Mater.* **2002**, *14*, 553–563.
- [46] C. Pereira, G. T. Kokotailo, R. J. Gorte, *J. Phys. Chem.* **1991**, *95*, 705–709.
- [47] F. A. Zhang, D. K. Lee, T. J. Pinnavaia, *Polym. Chem.* **2010**, *1*, 107–113.
- [48] A. Comotti, S. Bracco, M. Beretta, J. Perego, M. Gemmi, P. Sozzani, *Chem. - A Eur. J.* **2015**, *21*, 18209–18217.
- [49] S. Mochizuki, T. Kitao, T. Uemura, *Chem. Commun.* **2018**, *54*, 11843–11856.
- [50] K. Tajima, T. Aida, *Chem. Commun.* **2000**, *0*, 2399–2412.
- [51] M. Choluj, W. Bartkowiak, *Int. J. Quantum Chem.* **2019**, e25997.
- [52] M. Santoro, F. A. Gorelli, R. Bini, J. Haines, A. van der Lee, *Nat. Commun.* **2013**, *4*, 1557.
- [53] D. Scelta, M. Ceppatelli, M. Santoro, R. Bini, F. A. Gorelli, A. Perucchi, M. Mezouar, A. Van Der Lee, J. Haines, *Chem. Mater.* **2014**, *26*, 2249–2255.
- [54] M. Santoro, K. Dziubek, D. Scelta, M. Ceppatelli, F. A. Gorelli, R. Bini, J. M. Thibaud, F. Di Renzo, O. Cambon, J. Rouquette, et al., *Chem. Mater.* **2015**, *27*, 6486–6489.
- [55] G. Confalonieri, M. Fabbiani, R. Arletti, S. Quartieri, F. Di Renzo, J. Haines, et al., *Microporous Mesoporous Mater.* **2020**, *300*, 110163.
- [56] T. Bein, P. Enzel, *Angew. Chemie Int. Ed. English* **1989**, *28*, 1692.
- [57] G. F. McCann, G. J. Millar, G. A. Bowmaker, R. P. Cooney, *J. Chem. Soc. Faraday Trans.* **1995**, *91*, 4321–4328.
- [58] M. Sierka, U. Eichler, J. Datka, J. Sauer, *J. Phys. Chem. B* **1998**, *102*, 10468–10468.
- [59] E. Fois, A. Gamba, G. Tabacchi, *J. Phys. Chem. B* **1998**, *102*, 3974–3979.
- [60] R. Grau-Crespo, A. G. Peralta, A. R. Ruiz-Salvador, A. Gómez, R. López-Cordero, *Phys. Chem. Chem. Phys.* **2000**, *2*, 5716–5722.
- [61] X. Rozanska, R. A. Van Santen, F. Hutschka, J. Hafner, *J. Catal.* **2002**, *205*, 388–397.
- [62] C. O. Arean, M. R. Delgado, P. Nachtigall, H. V. Thang, M. Rubeš, R. Bulánek, P. Chlubná-Eliášová, *Phys. Chem. Chem. Phys.* **2014**, *16*, 10129–10141.
- [63] V. Pashkova, S. Sklenak, P. Klein, M. Urbanova, J. Dědeček, *Chem. - A Eur. J.* **2016**, *22*, 3937–3941.
- [64] G. Li, E. A. Pidko, *ChemCatChem* **2019**, *11*, 134–156.
- [65] M. Fischer, *Chem. - A Eur. J.* **2019**, *25*, 13579–13590.
- [66] M. Jaymand, *RSC Adv.* **2014**, *4*, 33935–33954.
- [67] P. Lotti, G. D. Gatta, M. Merlini, H.-P. Liermann, *Zeitschrift für Krist. - Cryst. Mater.* **2015**, *230*, 201–211.
- [68] J. L. Mackey, Z. Yang, K. N. Houk, *Chem. Phys. Lett.* **2017**, *683*, 253–257.
- [69] D. Walther, T. Döhler, K. Heubach, O. Klobes, B. Schweder, H. Görls, *Zeitschrift für Anorg. und Allg. Chemie* **1999**, *625*, 923–932.
- [70] P. D. Hustad, G. W. Coates, *J. Am. Chem. Soc.* **2002**, *124*, 11578–11579.
- [71] H. M. Jeong, J. H. Song, K. W. Chi, I. Kim, K. T. Kim, *Polym. Int.* **2002**, *51*, 275–280.
- [72] G. J. Domski, J. M. Rose, G. W. Coates, A. D. Bolig, M. Brookhart, *Prog. Polym. Sci.* **2007**, *32*, 30–92.
- [73] X. Shi, Y. Wang, J. Liu, D. Cui, Y. Men, Y. Li, *Macromolecules* **2011**, *44*, 1062–1065.
- [74] L. Cavallo, G. Guerra, P. Corradini, L. Resconi, R. M. Waymouth, *Macromolecules* **1993**, *26*, 260–267.
- [75] O. R. De Ballesteros, V. Venditto, F. Auriemma, G. Guerra, L. Resconi, R. Waymouth, A. L. Mogstad, *Macromolecules* **1995**, *28*, 2383–2388.
- [76] W. M. Meier, *Zeitschrift für Krist. - New Cryst. Struct.* **1961**, *115*, 439.
- [77] C. Baerlocher, L. B. McCusker, D. H. Olson, *Atlas of Zeolite Framework Types*, Elsevier, **2007**.
- [78] R. Arletti, A. Martucci, A. Alberti, L. Pasti, M. Nassi, R. Bagatin, *J. Solid State Chem.* **2012**, *194*, 135–142.
- [79] A. Martucci, L. Pasti, M. Nassi, A. Alberti, R. Arletti, R. Bagatin, R. Vignola, R. Sticca, *Microp. Mesoporous Mater.* **2012**, *151*, 358–367.
- [80] S. Blasioli, A. Martucci, G. Paul, L. Gigli, M. Cossi, C. T. Johnston, L. Marchese, I. Braschi, *J. Colloid Interface Sci.* **2014**, *419*, 148–159.
- [81] R. Arletti, L. Leardini, G. Vezzalini, S. Quartieri, L. Gigli, M. Santoro, J. Haines, J. Rouquette, L. Konczewicz, *Phys. Chem. Chem. Phys.* **2015**, *17*, 24262–24274.
- [82] R. Fantlini, R. Arletti, S. Quartieri, M. Fabbiani, S. Morandi, G. Martra, F. Di Renzo, G. Vezzalini, *Microporous Mesoporous Mater.* **2020**, *294*, 109892.
- [83] Y. Hu, G. Martra, J. Zhang, S. Higashimoto, S. Coluccia, M. Anpo, *J. Phys. Chem. B* **2006**, *110*, 1680–1685.
- [84] V. Bolis, C. Busco, S. Bordiga, P. Ugliengo, C. Lamberti, A. Zecchina, in *Appl. Surf. Sci.*, Elsevier, **2002**, pp. 56–70.
- [85] H. Hattori, P. Arudra, A. Abdalla, A. M. Aitani, S. S. Al-Khattaf, *Catal. Letters* **2020**, *150*, 771–780.
- [86] C. Pazè, B. Sazak, A. Zecchina, J. Dwyer, *J. Phys. Chem. B* **1999**, *103*, 9978–9986.
- [87] N. B. Colthup, L. H. Daly, S. E. Wiberly, *Introduction to Infrared and Raman Spectroscopy*, Academic Press, New York, **1975**.
- [88] G. Herzberg, *Molecular Spectra and Molecular Structure. II. Infrared and Raman Spectra of Polyatomic Molecules*, Van Nostrand Company, Princeton, New Jersey, US, **1962**.
- [89] L. Gigli, R. Arletti, G. Tabacchi, E. Fois, J. G. Vitillo, G. Martra, G. Agostini, S. Quartieri, G. Vezzalini, *J. Phys. Chem. C* **2014**, *118*, 15732–15743.
- [90] G. Tabacchi, G. Calzaferri, E. Fois, *Chem. Commun.* **2016**, *52*, 1195–1198.
- [91] E. Fois, G. Tabacchi, G. Calzaferri, *J. Phys. Chem. C* **2012**, *116*, 16784–16799.
- [92] W. Insuwan, K. Rangswatananon, J. Meeprasert, S. Namuangruk, Y. Surakhot, N. Kungwan, S. Jungsuttiwong, *Microporous Mesoporous Mater.* **2017**, *241*, 372–382.
- [93] M. Fischer, *J. Phys. Chem. C* **2020**, *124*, 5690–5701.
- [94] V. Martínez-Martínez, R. García, L. Gómez-Hortigüela, J. Pérez-Pariente, I. López-Arbeloa, *Chem. - A Eur. J.* **2013**, *19*, 9859–9865.
- [95] G. W. Coates, R. M. Waymouth, *J. Am. Chem. Soc.* **1991**, *113*, 6270–6271.
- [96] K. Nomura, Y. Hatanaka, H. Okumura, M. Fujiki, K. Hasegawa, *Macromolecules* **2004**, *37*, 1693–1695.
- [97] G. Confalonieri, S. Quartieri, G. Vezzalini, G. Tabacchi, E. Fois, T. J. Daou, R. Arletti, *Microp. Mesoporous Mater.* **2019**, *284*, 161–169.
- [98] F. Trudu, G. Tabacchi, E. Fois, *Am. Mineral.* **2019**, *104*, 1546–1555.
- [99] R. T. Mathers, G. W. Coates, *Chem. Commun.* **2004**, *10*, 422–423.
- [100] C. Prescher, V. B. Prakapenka, *High Press. Res.* **2015**, *35*, 223.
- [101] A. C. Larson, R. B. Von Dreele, **1994**, LAUR 86–748.
- [102] B. H. Toby, *J. Appl. Crystallogr.* **2001**, *34*, 210–213.
- [103] P. Thompson, D. E. Cox, J. B. Hastings, *J. Appl. Crystallogr.* **1987**, *20*, 79–83.
- [104] S. Grimme, *J. Comput. Chem.* **2006**, *27*, 1787–1799.
- [105] E. S. Fois, J. I. Penman, P. A. Madden, *J. Chem. Phys.* **1993**, *98*, 6352.
- [106] J. Klimeš, D. P. Tew, *J. Chem. Phys.* **2019**, *151*, 234108.
- [107] M. Fischer, W. J. Kim, M. Badawi, S. Lebegue, *J. Chem. Phys.* **2019**, *150*, 094102.
- [108] M. Fischer, F. O. Evers, F. Formalik, A. Olejniczak, *Theor. Chem. Acc.* **2016**, *135*, 257.
- [109] M. Fischer, M. R. Delgado, C. O. Areán, C. O. Duran, *Theor. Chem. Acc.* **2015**, *134*, 91.
- [110] H. Hay, G. Ferlat, M. Casula, A. P. Seitsonen, F. Mauri, *Phys. Rev. B* **2015**, *92*, 144111.
- [111] F. Trudu, G. Tabacchi, A. Gamba, E. Fois, *J. Phys. Chem. A* **2007**, *111*, 11626–37.
- [112] M. Abatal, A. R. Ruiz-Salvador, N. C. Hernández, *Microporous Mesoporous Mater.* **2020**, 109885.
- [113] E. Fois, G. Tabacchi, *Z. Kristallogr.* **2019**, *234*, 495–511.
- [114] G. Bandoli, D. Barreca, A. Gasparotto, R. Seraglia, E. Tondello, A. Devi, R. A. Fischer, M. Winter, E. Fois, A. Gamba, et al., *Phys. Chem. Chem. Phys.* **2009**, *11*, 5998.
- [115] E. Fois, G. Tabacchi, D. Barreca, A. Gasparotto, E. Tondello, *Angew. Chemie - Int. Ed.* **2010**, *49*, 1944–1948.
- [116] D. Barreca, E. Fois, A. Gasparotto, R. Seraglia, E. Tondello, G. Tabacchi, *Chem. - A Eur. J.* **2011**, *17*, 10864–10870.
- [117] C. Maccato, L. Bigiani, G. Carraro, A. Gasparotto, R. Seraglia, J. Kim, A. Devi, et al., *Chem. - A Eur. J.* **2017**, *23*, 17954–17963.
- [118] G. Tabacchi, M. Fabbiani, L. Mino, G. Martra, E. Fois, *Angew. Chemie Int. Ed.* **2019**, *58*, 12431–12434.
- [119] C. Deiana, E. Fois, G. Martra, S. Narbey, F. Pellegrino, G. Tabacchi, *ChemPhysChem* **2016**, *17*, 1956–1960.
- [120] D. Marx, J. Hutter, *Ab Initio Molecular Dynamics*, Cambridge University Press, Cambridge, **2009**.
- [121] R. Car, M. Parrinello, *Phys. Rev. Lett.* **1985**, *55*, 2471–2474.
- [122] D. Vanderbilt, *Phys. Rev. B* **1990**, *41*, 7892–7895.
- [123] N. Troullier, J. L. Martins, *Phys. Rev. B* **1991**, *43*, 1993–2006.
- [124] CPMD code, IBM Corp. 1990–2017, MPI für Festkörperforschung Stuttgart 1997–2001, **2017**.
- [125] W. Humphrey, A. Dalke, K. Schulten, *J. Mol. Graph.* **1996**, *14*, 33–38; b) M. D Hanwell, D. E. Curtis, D. C. Lonie, T. Vandermeersch, E. Zurek, G. R. Hutchison, *J. Cheminform.* **2012**, *4*, 17.

TOC graphics



The channel system of zeolite mordenite, highlighting the void-space architecture constituted by the 12-membered ring channel and the side pockets.

(Image created using the Database of Zeolite Structures, Structure Commission of the International Zeolite Association

<https://europe.iza-structure.org/IZA-SC/framework.php?STC=MOR>)